Nuclear Magnetic Resonance (NMR) Solution Structure, Dynamics, and Binding Properties of the Kringle IV Type 8 Module of Apolipoprotein(a)[†,‡]

Seth Chitayat,[§] Voula Kanelis,[||] Marlys L. Koschinsky,[§,⊥] and Steven P. Smith*[,§,#]

Department of Biochemistry, Queen's University, Kingston, Ontario K7L 3N6, Canada, Department of Biochemistry, University of Toronto, Toronto, Ontario M5S 1A8, Canada, Cardiovascular, Circulatory and Respiratory Research Group, Queen's University, Kingston, Ontario K7L 3N6, Canada, and Protein Function Discovery Group, Queen's University, Kingston, Ontario K7L 3N6, Canada

Received August 31, 2006; Revised Manuscript Received December 4, 2006

ABSTRACT: The plasma lipoprotein lipoprotein(a) [Lp(a)] comprises a low-density lipoprotein (LDL)-like particle covalently attached to the glycoprotein apolipoprotein(a) [apo(a)]. Apo(a) consists of multiple tandem repeating kringle modules, similar to plasminogen kringle IV (designated KIV_1−KIV_{10}), followed by modules homologous to the kringle V module and protease domain of plasminogen. The apo(a) KIV modules have been classified on the basis of their binding affinity for lysine and lysine analogues. The strong lysine-binding apo(a) KIV_{10} module mediates lysine-dependent interactions with fibrin and cell-surface receptors. Weak lysine-binding apo(a) KIV_7 and KIV_8 modules display a 2−3-fold difference in lysine affinity and play a direct role in the noncovalent step in Lp(a) assembly through binding to unique lysine-containing sequences in apolipoproteinB-100 (apoB-100). The present study describes the nuclear magnetic resonance solution structure of apo(a) KIV_8 and its solution dynamics properties, the first for an apo(a) kringle module, and compares the effects of ϵ-aminocaproic acid (ϵ-ACA) binding on the backbone and side-chain conformation of KIV_7 and KIV_8 on a per residue basis. Apo(a) KIV_8 adopts a well-ordered structure that shares the general tri-loop kringle topology with apo(a) KIV_6, KIV_7, and KIV_{10}. Mapping of ϵ-ACA-induced chemical-shift changes on KIV_7 and KIV_8 indicate that the same residues are affected, despite a 2−3-fold difference in ϵ-ACA affinity. A unique loop conformation within KIV_8, involving hydrophobic interactions with Tyr^{40}, affects the positioning of Arg^{35} relative to the lysine-binding site (LBS). A difference in the orientation of the aromatic side chains comprising the hydrophobic center of the LBS in KIV_8 decreases the size of the hydrophobic cleft compared to other apo(a) KIV modules. An exposed hydrophobic patch contiguous with the LBS in KIV_8 and not conserved in other weak lysine-binding apo(a) kringle modules may modulate specificity for regions within apoB-100. An additional ligand recognition site comprises a structured arginine−glycine−aspartate motif at the N terminus of the KIV_8 module, which may mediate Lp(a)/apo(a)−integrin interactions.

Lipoprotein(a) [Lp(a)][1] is a plasma lipoprotein comprising a low-density lipoprotein (LDL)-like moiety that is attached to the glycoprotein apolipoprotein(a) [apo(a)] by a single disulfide bond (*1*, *2*). The LDL moiety of Lp(a) is similar to the plasma-derived LDL both in lipid composition and in the presence of apolipoprotein B-100 (apoB-100) (*3*). As such, the apo(a) component likely confers the unique structural and functional properties that have been attributed to Lp(a). Apo(a) contains tandem repeats of a sequence that closely resembles plasminogen kringle IV (∼75−85% similarity), followed by sequences that are highly homologous to the kringle V and protease domains of plasminogen (*4*). On the basis of the amino acid sequence, apo(a) contains 10 distinct subclasses of plasminogen kringle IV-like domains (KIV_1−KIV_{10}) (*4*). Apo(a) KIV types 1 and 3−10 are present as single copies, while the kringle IV type 2 domain (KIV_2) is present in a variable number of identically repeated copies and is the molecular basis for the observed isoform size heterogeneity of Lp(a) (*5*, *6*).

[†] This research was supported by the Heart and Stroke Foundation of Ontario Grant-in-Aid funding to S.P.S. (T 5871) and a Canadian Institutes of Health Research Operating Grant to M.L.K. (MOP-11271). The infrastructure used in these studies was funded by the Canadian Foundation for Innovation and the Ontario Innovation Trust. S.C. is a recipient of an E.G. Bauman Fellowship, and V.K. is a recipient of a Cystic Fibrosis Fellowship. M.L.K. is a Heart and Stroke Foundation of Ontario Career Investigator, and S.P.S. is a Canadian Institutes of Health Research New Investigator.

[‡] ^1H, ^{13}C, and ^{15}N resonance assignments of apo(a) KIV_8 have been deposited in the BioMagResBank (BMRB) as accession number 7032. The coordinates for apo(a) KIV_8 have been deposited in the Protein Data Bank as accession number 2FEB.

* To whom correspondence should be addressed. Telephone: (613) 533-3188. Fax: (613) 533-2497. E-mail: sps1@post.queensu.ca.

[§] Department of Biochemistry, Queen's University.

[||] Department of Biochemistry, University of Toronto.

[⊥] Cardiovascular, Circulatory and Respiratory Research Group, Queen's University.

[#] Protein Function Discovery Group, Queen's University.

[1] Abbreviations: AMCHA, *trans*-(aminomethyl)cyclohexanecarboxylic acid; apo(a), apolipoprotein(a); apoB-100, apolipoprotein B-100; DTT, dithiothreitol; IPTG, isopropyl-β-D-thiogalactopyranoside; ϵ-ACA, ϵ-aminocaproic acid; KIV, kringle IV module; LB, Luria Bertani; LBS, lysine-binding site; LDL, low-density lipoprotein; Lp(a), lipoprotein(a); NMR, nuclear magnetic resonance; NOE, nuclear Overhauser effect; rmsd, root-mean-square deviation.

10.1021/bi061814g CCC: $37.00
Published on Web 01/31/2007

While a physiological role of Lp(a) has yet to be determined, numerous epidemiological studies have identified elevated plasma Lp(a) concentrations as a risk factor for the development of atherosclerotic disorders, including coronary heart disease (reviewed in refs *7* and *8*). The unique structure of Lp(a) has suggested both a proatherogenic role, because of its similarity to LDL, and a prothrombotic/antifibrinolytic role, on the basis of the resemblance of apo(a) to plasminogen (*9*−*11*). It is generally accepted that the assembly of LDL and apo(a) into the Lp(a) particle is a two-step process in which a noncovalent interaction between apo(a) and apoB-100 (*12*−*16*) precedes disulfide bond formation between a free cysteine residue (Cys^{4507}) within the KIV_9 module of apo(a) (*1*, *2*) and a cysteine residue of apoB-100, the identify of which remains to be definitively identified. Biochemical and biophysical studies have implicated Cys^{3734} of apoB-100 in the covalent step (*17*, *18*), while more recent site-directed mutagenesis studies suggested that Cys^{4326} in apoB-100 was required for Lp(a) formation (*19*, *20*).

In vitro studies have shown that the noncovalent step in Lp(a) assembly can be inhibited by the addition of lysine, lysine analogues, arginine, proline, and phenylalanine (*15*, *21*−*23*) and that the weak lysine-binding sites (LBS) present within the KIV_5−KIV_8 region of apo(a) are likely involved in mediating this interaction (*16*, *21*, *22*, *24*, *25*). Apo(a) KIV_6 (*15*, *22*, *26*), KIV_7 (*12*, *15*, *16*, *26*), and KIV_8 (*12*, *15*) modules have been implicated in the noncovalent step, and recombinant constructs of each have been shown to display moderate to weak affinities for the lysine analogue ϵ-aminocaproic acid (ϵ-ACA) (*12*, *27*), when compared to the high-affinity ϵ-ACA-binding KIV_{10} module [dissociation constant (K_d) = 20 μM] (*24*, *28*−*31*). KIV_6 and KIV_7, whose structures have been previously determined (*27*, *32*), display similar ϵ-ACA affinities ($K_d \sim 0.2$−0.3 mM), while KIV_8 has a 2−3-fold lower affinity (*12*). Mutagenesis studies ruled out a role for KIV_6 in the initial noncovalent step, while KIV_7 and KIV_8 were both required for maximally efficient noncovalent and covalent Lp(a) assembly and recognized unique lysine-containing sequences in apoB-100 of the LDL-like moiety (*12*, *14*).

A recent role for apo(a) in integrin-mediated cellular functions has also emerged. A lysine-dependent interaction between apo(a) and the Mac-1 integrin promoted endothelial cell adhesion and migration (*33*). Lp(a) also decreased platelet aggregation through an interaction between the fibrinogen receptor and the sole arginine−glycine−aspartate (RGD) motif of apo(a), which is located at the N terminus of the KIV_8 module (*34*).

In this study, we describe the nuclear magnetic resonance (NMR) solution structure of the KIV_8 module of apo(a), which has a similar overall fold to structures of apo(a) KIV_6 (*27*), KIV_7 (*32*), and KIV_{10} (*29*, *30*). Analysis of the dynamics properties of KIV_8 is presented, the first for an apo(a) kringle module, and using backbone chemical-shift mapping, we show that there is no significant difference in the residues of KIV_7 and KIV_8 affected by ϵ-ACA binding, despite a 2−3-fold difference in the binding affinity. Notable differences in KIV_8 are observed in the side-chain orientations of several aromatic residues, both within and adjacent to the LBS, and appear to alter the cationic and hydrophobic centers of the LBS. These observations provide a structural rationale for the differential modes of apoB-100 recognition by KIV_7 and KIV_8. In addition, the structure reveals that the RGD motif within KIV_8 is structured and indeed accessible for the interaction with integrin target proteins.

MATERIALS AND METHODS

Cloning of Apo(a) KIV_8/pET-16b and KIV7/pET-16b. The upstream and downstream primers GGACTGACATATG-GCACAACTGAAAACAGCAC and CCCATATGTTAG-ACACTCGATTCTGTCACTGGACATCGTGTCAGGTT-GC, respectively, were used in a polymerase chain reaction (PCR) amplification with the KIV_8/prK5 plasmid[2] to generate a 300 base pair (bp) fragment encoding apo(a) KIV_8 with 5′ and 3′ *Nde*I restriction sites (underlined). The resulting fragment was subcloned and ligated into the *Eco*RV site of BlueScript (Strategene) using T4 DNA ligase (Invitrogen) and transformed into *Escherichia coli* DH5α. The ligation mixture was plated on Luria Bertani (LB)−ampicillin plates containing isopropyl-β-D-thiogalactopyranoside (IPTG) and X-galactose. Plasmids were extracted from white colonies and digested with *Nde*I to excise the 300 bp fragment. The digested fragment was inserted into the *Nde*I site of the cloning region of a pET-16b expression vector (Stratagene) using T4 DNA ligase (Invitrogen). The directionality and sequence of the insert was confirmed by DNA sequencing, and the plasmid was transformed into the *E. coli* BL21 (DE3) strain for expression.

The apo(a) KIV_7/pET-16b expression plasmid was constructed in a manner similar to the apo(a) KIV_8/pET-16b expression plasmid, with the exception that the KIV_7/prk5 plasmid and the *Nde*I-containing (underlined) up- and downstream primers GGACTGACATATGGCACCAACG-GAGCAAAGCCC and GGCATATGTTAGAGAGTTGAT-TCCATCACTGGAC were used to generate the 300 bp fragment encoding apo(a) KIV_7.

Protein Expression and Purification. The expression, refolding, and purification of recombinant apo(a) KIV_8 and KIV_7 were performed using a modified protocol by Becker et al. (*12*). Transformed cells were grown in LB media supplemented with 100 μg/L ampicillin in a 2.8 L Fernbach flask at 37 °C with shaking to an OD_{600} of 0.75. IPTG was added to a final concentration of 1 mM, and growth was continued for an additional 6 h at 30 °C. The cells were harvested by centrifugation, resuspended in a volume of buffer A (20 mM Tris-HCl at pH 7.9, 500 mM NaCl, and 5 mM imidazole) equal to 10 times their packed weight, and disrupted by sonication (4 × 30 s) on ice. Cell debris was removed by centrifugation for 20 min at 48000*g* in a Beckman 25.5 rotor. The supernatant solution was discarded; the pellet was resuspended in buffer A to 5 times its packed weight; and the sonication and centrifugation steps were repeated. The pellet was resuspended, sonicated (4 × 30 s) in buffer B [20 mM Tris-HCl at pH 7.9, 500 mM NaCl, 5 mM imidazole, 0.5% Triton, and 5 mM dithiothreitol (DTT)] and left to rock at 4 °C for 3 days. The suspension was increased to 5 times its original volume in buffer A; the concentrations of oxidized and reduced glutathione were added to a final concentration of 1.25 mM; and the sample was agitated overnight at 4 °C. The supernatant was applied to a column packed with 2 mL of Ni^{2+}-chelating sepharose

[2] M. L. Koschinsky, unpublished data.

beads (Amersham Pharmacia Biotech) equilibrated with buffer A. The column was washed with 10 mL of buffer A containing 60 mM imidazole. The bound protein was eluted with buffer A containing 1 M imidazole in 1 mL fractions. Fractions containing protein were determined by the Bradford assay and sodium dodecyl sulfate−polyacrylamide gel electrophoresis (SDS−PAGE), pooled, and loaded onto a Hi-Load 16/60 Superdex 75 size-exclusion column (Amersham Pharmacia Biosciences) equilibrated with 20 mM Tris-HCl at pH 7.9 and 25 mM NaCl. Elution fractions (3 mL) were collected using the same buffer. Fractions containing protein were pooled and concentrated using an Amicon stirred cell (Millipore Corporation) with a 1 kDa membrane at 4 °C under pressure from nitrogen gas. The pH of the sample was adjusted to 3.5 using trifluoracetic acid, filtered using a 0.45 μm nylon acrodisc filter, and loaded on a Vydar C18 protein and peptide column attached to a Beckman high-performance liquid chromatograph (HPLC). Apo(a) KIV_8 and KIV_7 eluted in 34 and 30% acetonitrile treated with 0.05% trifluoroacetic acid, respectively. Acetonitrile was removed from the samples using a Savant Speed Vac Concentrator, and the samples were flash-frozen in liquid nitrogen and lyophilized. Dried protein was stored at −20 °C.

Uniformly ^{15}N- and ^{13}C/^{15}N-labeled apo(a) KIV_8 and KIV_7 were expressed, refolded, and purified in a manner similar to that of the unlabeled protein, with the exception that a 5 mL bacterial culture of LB was used to inoculate 50 mL of M9 minimal media containing ^{14}N-NH_4Cl and ^{12}C-glucose. At an OD_{600} of 1.1, 10 mL was used to inoculate 1 L of M9 minimal media containing 1 g/L ^{15}N-NH_4Cl for uniform ^{15}N labeling and 2 g/L ^{13}C-glucose and 1 g/L ^{15}N-NH_4Cl for uniform ^{13}C/^{15}N labeling (Cambridge Isotope Laboratories). At induction, ^{15}N- and ^{13}C/^{15}N-labeled growths were supplemented with 10 mL of ^{15}N-Bio-Express-1000 media or 10 mL of ^{13}C/^{15}N-Bio-Express-1000 media (Cambridge Isotope Laboratories), respectively, and 50 μg/L ampicillin. Growth was continued for 14 h after IPTG induction at 30 °C. NMR samples were prepared in 20 mM Tris-HCl at pH 7.2 in 90% H_2O/10% D_2O (v/v) to a final protein concentration of 1 mM.

NMR Spectroscopy. All NMR experiments were performed at 25 °C on Varian 600 and 800 MHz spectrometers equipped with pulse field-gradient triple-resonance cryoprobes. Sequential backbone and side-chain assignments were determined using ^{1}H−^{15}N heteronuclear single-quantum coherence (HSQC) (*35*), HNCACB (*36*), CBCACONH (*37*), HNHA (*38*, *39*), C(CO)NH−total correlation spectroscopy (TOCSY) and HC(CO)NH−TOCSY (*40*), and HCCH−TOCSY (*41*) experiments. ^{1}H, ^{13}C, and ^{15}N resonance assignments of apo(a) KIV_8 have been deposited in the BMRB (accession number 7032). Interproton distances of apo(a) KIV_8 were measured from three-dimensional ^{15}N-edited nuclear Overhauser effect spectrometry (NOESY)−HSQC (*42*), ^{13}C-edited NOESY−HSQC (*43*), and ^{13}C-aromatic NOESY (*44*) datasets with mixing times of 150 ms. All data were processed and analyzed using NMRPipe (*45*) and NMRView (*46*), respectively.

^{15}N T_1, ^{15}N T_2, and {^{1}H}−^{15}N nuclear Overhauser effect (NOE) values for the apo(a) KIV_8 were measured at 600 MHz using experiments similar to those described by Farrow et al. (*47*). Longitudinal delays of 10, 20, 40, 80, 320, and 640 ms (T_1) and Carr−Purcell−Meiboom−Gill (CPMG) delays of 10, 30, 50, 70, 90, 110, 150, and 190 ms (T_2) were used in the acquisition of the data. Steady-state heteronuclear {^{1}H}−^{15}N NOE data were obtained with and without 3 s of proton saturation and a total recycle delay of 7 s. NOE values were extracted as the ratio of peak intensities with and without proton saturation for 73 well-resolved resonances. Rate analysis functions in NMRView 5.0.4 were used to analyze the T_1 and T_2 decay rates, which were computed using the two-parameter model using CurveFit (*48*) for 70 well-resolved resonances. The isotropic rotation correlation time (τ_m) was approximated using the ratio of R_2/R_1, and average R_2 and R_1 values were computed for only well-resolved resonances.

Structure Calculation. Structures of apo(a) KIV_8 were generated using the simulated annealing protocol in CNS 1.1 with 20 000 molecular dynamic steps and 10 cycles of 1000 minimization steps (*49*). Interproton distances were calibrated for all proton pairs using maximum and minimum NOE intensities for known distances ($d_{\beta N}$, $d_{\alpha N}$, and d_{NN}) in regions comprising the loop or extended structure. A total of 3044 NOE-derived distance restraints were obtained for the structure calculation, including 2098 short-range (intraresidue and sequential), 348 medium-range ($1 < |i - j| \leq 5$), and 598 long-range ($|i - j| > 5$) distance restraints. Additional restraints were introduced corresponding to the well-conserved kringle module disulfide bond pattern (Cys^1−Cys^{78}, Cys^{22}−Cys^{61}, and Cys^{50}−Cys^{73}). Backbone dihedral angle restraints (ψ angle) for six residues, Cys^1, Tyr^2, Cys^{61}, Trp^{70}, Thr^{76}, and Arg^{77}, located in secondary-structure elements, were obtained from analysis of $^{13}C^{\alpha}$, $^{13}C^{\beta}$, $^{13}C'$, $^1H^{\alpha}$, and ^{15}N chemical shifts using TALOS (*50*). An additional 43 ϕ angle restraints were used from HNHA-derived $^3J_{HN\alpha}$ coupling constants (*51*). The 20 lowest energy structures with no distance violations greater than 0.3 Å and no angle violations greater than 5° were accepted into the final ensemble, and the quality of the structures was evaluated using PROCHECK and MOLMOL (*52*, *53*). All figures representing structures were generated using MOLMOL (*53*) or PyMOL (*54*).

NMR-Based ϵ-ACA Titrations. Titrations of 0.21 mM ^{15}N-apo(a) KIV_8 or 0.21 mM ^{15}N-apo(a) KIV_7 with incremental additions of ϵ-ACA were monitored using 2D ^{1}H−^{15}N HSQC spectra recorded at 25 °C and 600 MHz. Sequential additions of ϵ-ACA giving rise to a total concentration of 200 μM, 800 μM, 1.5 mM, 3 mM, 6 mM, 10 mM, and 20 mM were added to apo(a) KIV_8 and 36 μM, 100 μM, 180 μM, 240 μM, 360 μM, 540 μM, 720 μM, 1.5 mM, 2.5 mM, 5 mM, and 10 mM were added to apo(a) KIV_7. Sample buffer conditions were 20 mM Tris-HCl at pH 7.2. The data were processed and analyzed using NMRPipe and NMRView 5.2.2, respectively (*45*, *46*), and dissociation constant (K_d) values were interpolated from plots of the chemical-shift change as a function of the ϵ-ACA concentration.

Intrinsic Tryptophan Fluorescence Spectroscopy. Effects on the intrinsic tryptophan fluorescence properties of apo(a) KIV_7 and apo(a) KIV_8 by a variety of amino acids were monitored using a Fluorolog-3 spectrometer (Horiba Jobin-Yvon). Incremental additions of glycine, ϵ-ACA, and L-amino acids, glutamine, proline, lysine, or arginine, from 1 M stock solutions were made to either 200 nM apo(a) KIV_7 or 200 nM apo(a) KIV_8, using excitation and emission wavelengths of 280 and 340 nm, respectively. The amino

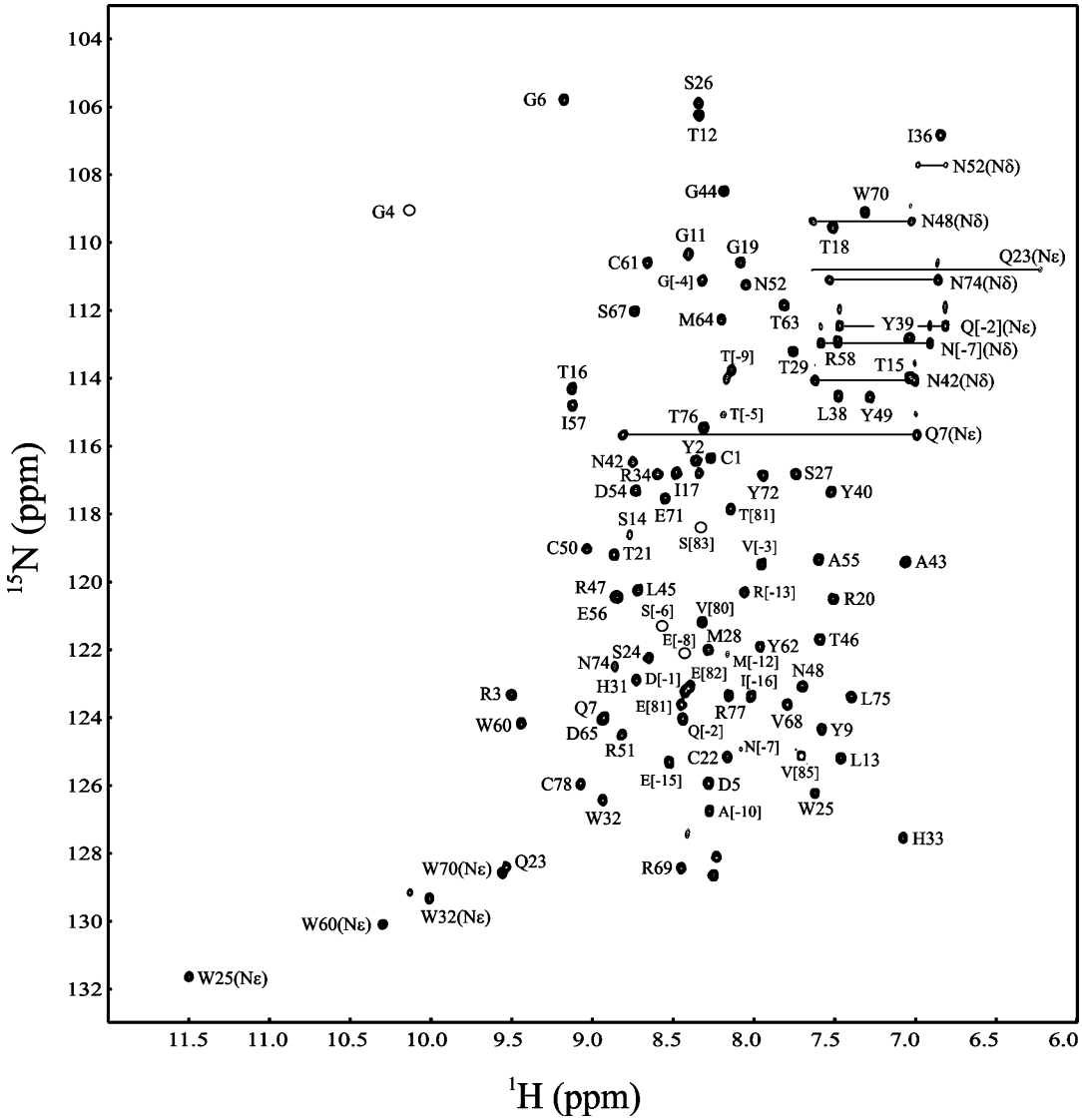

FIGURE 1: ^{1}H−^{15}N HSQC spectrum of 1 mM uniformly ^{13}C/^{15}N-labeled apo(a) KIV_8 at pH 7.2 and 25 °C recorded at 600 MHz. Resonances for backbone and side-chain amide protons that have been assigned are labeled with a one-letter code for amino acid type, followed by the position in sequence. Labels for side-chain resonances indicate the side-chain amide nitrogen atom in parantheses. Resonances of chemically equivalent side-chain amides of aspargine and glutamine residues are connected by horizontal lines and labeled accordingly.

acid and protein solution contained 20 mM Tris-HCl at pH 7.9 and 25 mM NaCl. The data were plotted and analyzed using SigmaPlot to obtain K_d values.

RESULTS

Resonance Assignments and the Solution Structure of Apo-(a) KIV_8. The assignment of backbone and side-chain ^{1}H, ^{15}N, and ^{13}C resonances of apo(a) KIV_8 was completed using standard multidimensional heteronuclear NMR techniques. In total, 94% of the expected backbone (Figure 1) and 91% of the side-chain resonances were assigned for the 102-residue construct comprising residues 3867−3962 of apo(a) (*4*) and a N-terminal deca-histidine tag. Backbone amide proton resonances of two N-terminal interkingle residues ($Gly^{[-15]}$ and $His^{[-13]}$) and four core residues (Ser^{8}, Arg^{10}, Arg^{35}, and Cys^{73}) were not observed in the ^{1}H−^{15}N HSQC spectrum, indicating that these residues occupy regions of the protein module that are exposed to the solvent.

NMR structures were calculated using 3044 NOE-derived distance restraints and 43 backbone ϕ and 6 ψ dihedral angle restraints obtained as described in the Materials and Methods. Using an extended starting model of apo(a) KIV_8, 133 structures were accepted from the 200 total generated structures based on the fact that they had no distance restraint violations greater than 0.3 Å and no dihedral angle restraint (ϕ and ψ) violations greater than 5°. From these accepted structures, the 20 lowest energy structures were selected for further analysis, and a summary of structural statistics is shown in Table 1. An average structure from this ensemble was calculated and minimized against experimental restraints.

KIV_8 adopts the typical tri-loop kringle fold, comprising two short β sheets and several loops and turns (Figure 2). A backbone superposition of the 20 lowest energy NMR structures, shown in Figure 2A, indicates that KIV_8 is well-defined by the NMR data, with the exception of a loop region comprising residues Gly^{4}−$Gly^{11}$and the N- and C-interkringle regions, defined by $Ile^{[-17]}$−$Asp^{[-1]}$ and $Pro^{[79]}$−$Val^{[102]}$, respectively. The lack of medium- and long-range NOEs associated with these regions suggest that they are disordered in solution. The root-mean-square deviation (rmsd) from the

Table 1: Structural Statistics for 20 Structures

restraints used in the structure calculation[a]	
number of distance restraints	
intraresidue	1421
inter-residue sequential (i, $i+1$)	677
inter-residue medium range ($1 < \|i-j\| < 5$)	348
long range ($\|i-j\| \geq 5$)	598
total	3044
rmsd values from distance restraints (Å)	0.0081 ± 0.0008
number of torsion angle restraints (ϕ and ψ)	49
geometric statistics	
rmsd values from idealized geometry	
bonds (Å)	0.0020 ± 0.00011
angles (deg)	0.348 ± 0.016
improper (deg)	0.186 ± 0.016
coordinate precision	
rmsd values from the minimized average structure[b] (Å)	
backbone atoms	0.764 ± 0.07
all heavy atoms	1.31 ± 0.11
Ramachandran analysis	
most favored region (%)	48
additionally allowed region (%)	36
generously allowed region (%)	11.3
disallowed regions (%)	3.5

[a] None of these structures exhibited distance violations of >0.3 Å or dihedral angles >5°. [b] The coordinate precision is defined as the average atomic rmsd values between the 20 structures and the minimized average structure. The reported values are for residues Cys^{1}−Cys^{78}.

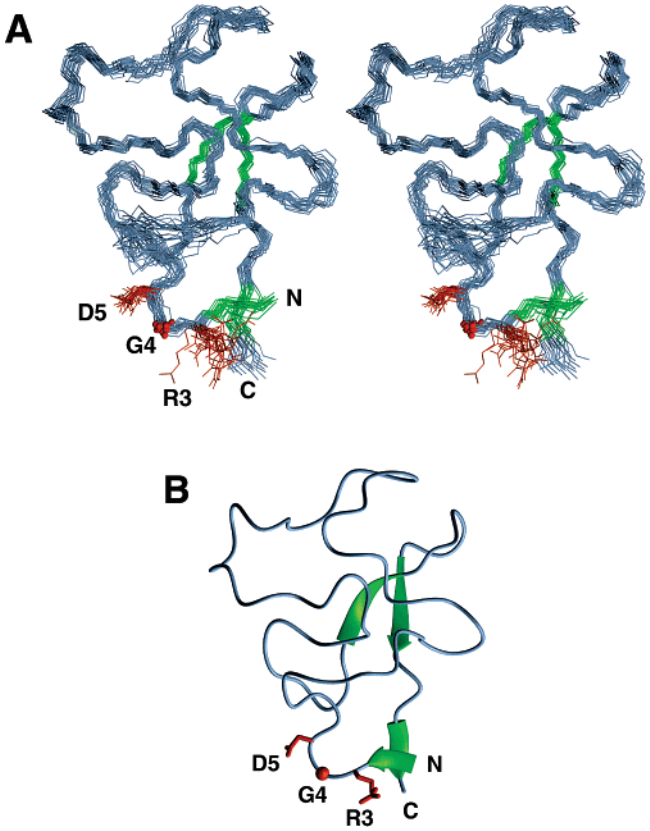

FIGURE 2: Apo(a) KIV_8 structure. (A) Stereoview representation of the backbone superposition (N, Cα, and C′ atoms) of the 20 lowest energy NMR structures and (B) ribbon diagram of the minimized average structure of the apo(a) KIV_8 module (residues Cys^{1}−Cys^{78}). The backbone of the residues found within two short β sheets are colored green and indicated by arrows in the minimized average structure. The side chains of the RGD motif are colored red and labeled using a one-letter code for amino acid type, followed by the position in sequence.

minimized average structure for the well-defined core of the ensemble, defined by residues Cys^{1}−Cys^{78}, is 0.764 ± 0.07 Å for the backbone atoms and 1.31 ± 0.11 Å for all heavy atoms. Ramachandran analysis in PROCHECK−NMR (*52*) indicated that 95% of all residues comprising the core region of KIV_8 fell within the allowed regions of ϕ and ψ space. The overall fold of apo(a) KIV_8 is similar to previously solved apo(a) kringle module structures, including the weak lysine-binding KIV_6 (*27*) and KIV_7 (*32*) modules and the high-affinity lysine-binding apo(a) KIV_{10} module (*29*). An antiparallel β sheet (Trp^{60}−Tyr^{62} and Trp^{70}−Tyr^{72}) and a parallel β sheet (Cys^{1}−Tyr^{2} and Thr^{76}−Arg^{77}) form the secondary-structure elements of KIV_8, while the remainder of the protein module comprises several loops and turns. KIV_8 lacks the 3_{10} helix observed in the apo(a) KIV_6 solution structure (*27*), which is also absent in the crystal structure of apo(a) KIV_7 (*32*).

Solution Dynamics of Apo(a) KIV$_8$. To investigate the backbone dynamic properties of KIV_8, the steady-state $\{^1H\}$−^{15}N NOE and longitudinal ^{15}N T_1 and transverse ^{15}N T_2 relaxation time constants were measured (Figure 3). Quantification of peak intensities was possible for 73 of the 88 total H^N backbone resonances from the $\{^1H\}$−^{15}N NOE dataset and 70 of the 88 total H^N backbone resonances in the ^{15}N T_1 and ^{15}N T_2 datasets. A partial overlap or weak signal precluded reliable quantification of the remaining H^N backbone resonances. The average $\{^1H\}$−^{15}N NOE value for residues Cys^{1}−Cys^{78} inclusive is 0.762, a value similar to that previously observed for the kringle 1 (KI) module of human plasminogen in the absence and presence of ε-ACA (*55*), and implies that the core of the apo(a) KIV_8 module is well-ordered. These NOE values are consistent with our experimental ^{15}N T_1 and ^{15}N T_2 values, which have averages for the core region of 569 and 78.1 ms, respectively. Very little deviation from these values is observed within the core region, suggesting that the relaxation properties of the molecule are governed by the overall diffusion tensor. Residues comprising the N-terminal interkringle region ($Ile^{[-17]}$−$Asp^{[-1]}$), Thr^{97}, Val^{102} at the extreme C termini, and Gly^{11} within the core region of apo(a) KIV_8 display smaller than average T_1/T_2 ratios, indicating increased mobility within these regions (parts B and C of Figure 3). Further, significantly reduced $\{^1H\}$−^{15}N NOE values are observed for these regions ($Ile^{[-17]}$−$Asp^{[-1]}$, Gly^{11}, and $Pro^{[79]}$−$Val^{[102]}$), indicating that they are undergoing motion on the subnanosecond time scale (Figure 3A). These observations are consistent with the lack of observed medium- and long-range NOEs within these regions and, in the case of Gly^{11}, backbone amide protons of proximal residues (Ser^{8} and Arg^{10}) undergoing exchange with the solvent.

An isotropic correlation time (τ_m) of 7.23 ns was estimated for the core region apo(a) KIV_8 from ^{15}N T_1 and ^{15}N T_2 values (*56*). This value is similar to the estimated τ_m of 7.97 ns for the amino-terminal kringle module of the urokinase-type plasminogen activator (*57*) and somewhat larger than those for the plaminogen kringle 1 (apo form, 5.91 ns; ε-ACA-bound form, 5.23 ns) (*55*) and 2 [*trans*-(aminomethyl)-cyclohexanecarboxylic acid (AMCHA)-bound form, 4.49 ns] (*58*). No aggregation was observed during size-exclusion chromatographic analysis of the purified apo(a) KIV_8, and

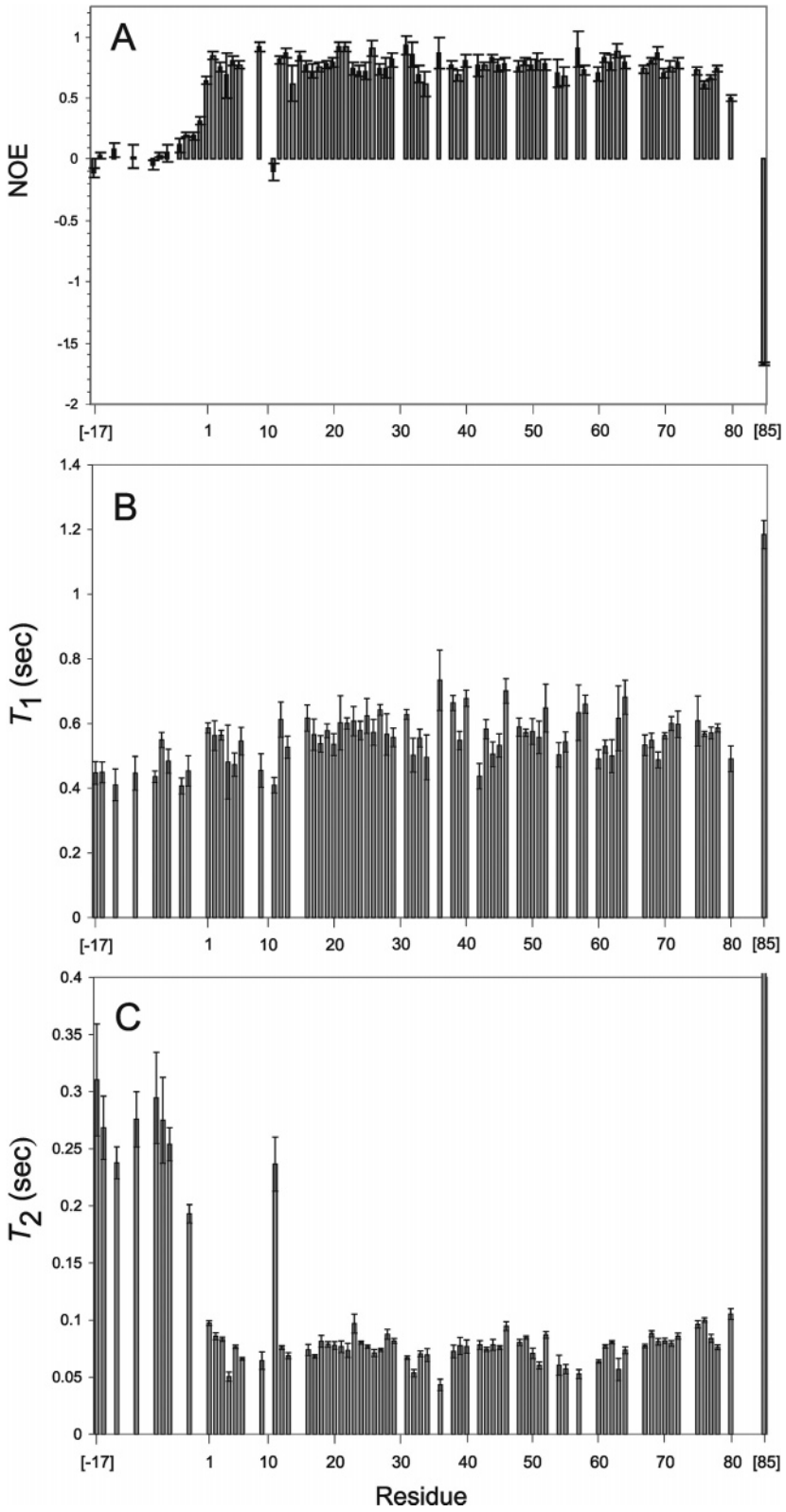

FIGURE 3: Plots of (A) NOE, (B) T_1, and (C) T_2 values as a function of the residue number for apo(a) KIV_8 at 14.1 T.

the ^{1}H line widths were not indicative of higher oligomeric species. However, we cannot rule out the possibility that a monomer−dimer equilibrium exists. Overall, the NMR relaxation results do suggest that the apo(a) KIV_8 construct is stable and ordered, with the exception of the N- and C-terminal interkringle regions and a region comprising Gly^{11}, data which is consistent with the NOE-based NMR solution structure of the apo(a) KIV_8 module described above.

ϵ-ACA and Amino-Acid-Binding Properties of Apo(a) KIV_7 and KIV_8. Although both apo(a) KIV_7 and KIV_8 modules have been identified as weak lysine-binding kringle modules (*12*, *15*, *16*), KIV_8 displays a 2−3-fold lower affinity for lysine analogue ϵ-ACA, despite the 84% sequence identity

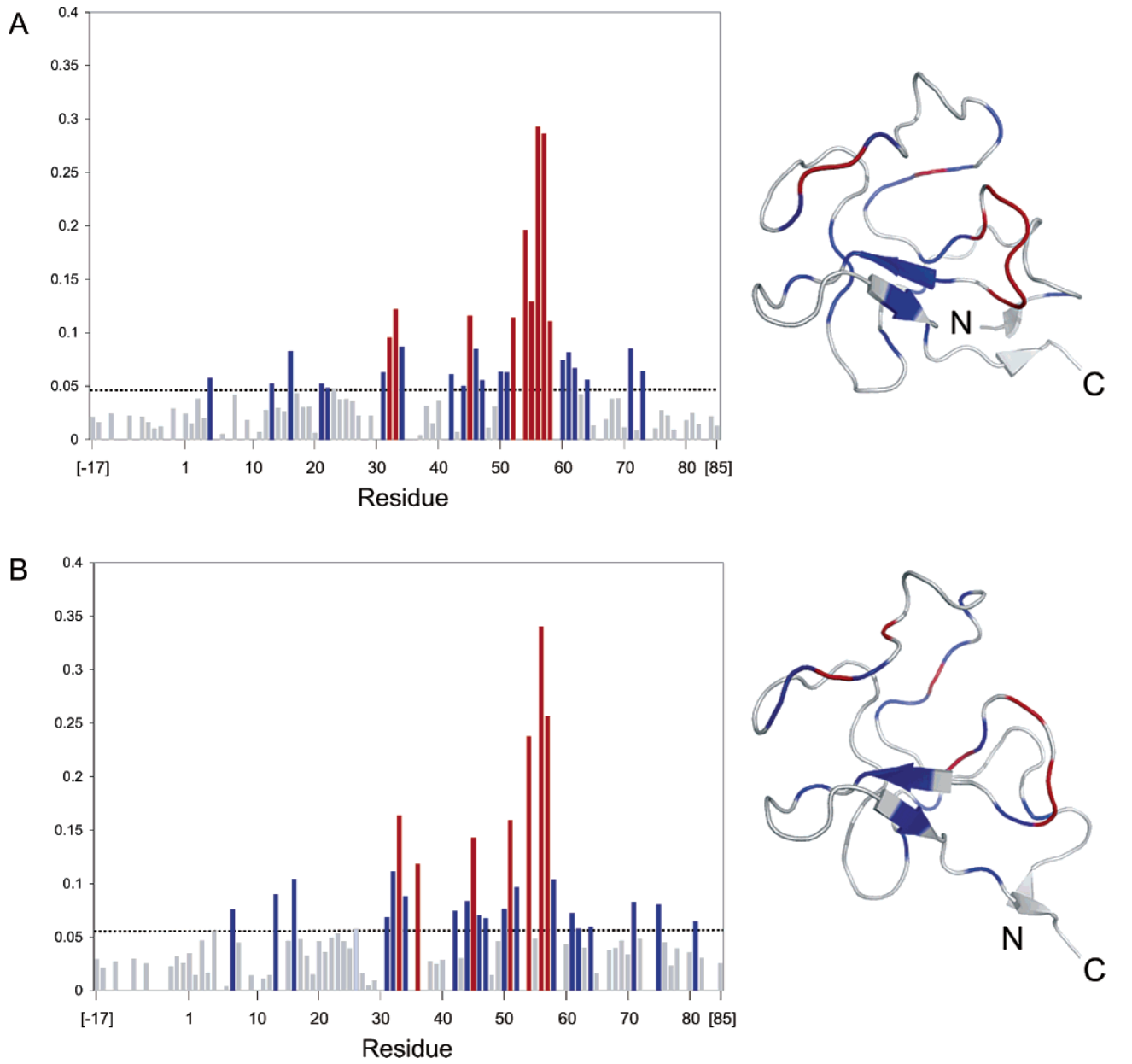

FIGURE 4: Plot of ϵ-ACA-induced average amide chemical-shift changes ($\Delta\delta$) along the sequence and on the backbone ribbon diagram of (A) apo(a) KIV_7 and (B) apo(a) KIV_8. The average chemical-shift changes were calculated using the formula $\Delta\delta = [(0.17\Delta\delta_N)^2 + (\Delta\delta_{HN})^2]^{1/2}$ (*61*). Red bars in the histograms and red-colored regions on the backbone ribbon diagrams indicate residues that exhibit chemical-shift changes exceeding the average chemical-shift change by greater than 1 standard deviation [>0.0993 ppm for apo(a) KIV_7 and >0.1154 ppm for apo(a) KIV_8]. Blue bars and blue-colored regions identify those residues that undergo chemical-shift changes greater than the average chemical-shift change but less than 1 standard deviation above the average [>0.0476 ppm for apo(a) KIV_7 and >0.0592 ppm for apo(a) KIV_8]. Black dashed lines represent the average chemical-shift change. The N and C termini are labeled in the backbone ribbon diagrams.

shared by these two modules (*12*). In an attempt to identify differences in ϵ-ACA-induced conformational changes between KIV_7 and KIV_8, we used 2D heteronuclear NMR-based ϵ-ACA titration studies.

Several backbone amide resonances from KIV_7 and KIV_8 displayed fast exchange on the NMR time scale upon titration with ϵ-ACA (see the Supporting Information), an observation consistent with the previously reported fluorescence-derived dissociation constants (K_d) for the KIV_7−ϵ-ACA (217 μM) and KIV_8−ϵ-ACA (800 μM) interactions (*12*). Quantification of these ϵ-ACA-induced backbone H^N and ^{15}N chemical-shift changes afforded the identification and comparison of residues whose local environments were affected upon binding of ϵ-ACA. As shown in Figure 4, those residues displaying significant (greater than 1 standard deviation above the average chemical-shift change; red bars) and notable chemical-shift changes (greater than the average chemical-shift change but less than 1 standard deviation above the average; blue bars) were similar for both the apo(a) KIV_7 and KIV_8 modules. When residues displaying prominent ϵ-ACA-induced changes were mapped on the backbone of their respective modules, they include residues of the anionic (KIV_7, Asp^{54}; KIV_8, Glu^{56}) and hydrophobic (KIV_7, Trp^{60} and Tyr^{62}; KIV_8, Tyr^{62}) centers of the LBS and those that are adjacent to the LBS of each module (KIV_7, His^{31}−Gln^{34}, Asn^{42}, and Gly^{44}−Arg^{47}; KIV_8, Cys^{50}−Arg^{58},

Table 2: Amino Acid Binding Affinities of Apo(a) KIV_7 and KIV_8[a]

	K_d (mM)			
	ϵ-ACA	L-lysine	L-arginine	L-proline
KIV_7	0.291	2.55	2.49	NC[b]
KIV_8	0.655	7.55	5.75	NC

[a] Apo(a) KIV_7 and KIV_8 were titrated with the indicated amino acids, and the protein intrinsic fluorescence was recorded. K_d values were obtained as described in the Materials and Methods. [b] No signifcant change in fluorescence was observed.

Cys[61], and Glu[71]). In addition, the side-chain indole groups of Trp[60] and Trp[70] in the LBS of both KIV_7 and KIV_8 display notable chemical-shift changes upon incremental additions of ϵ-ACA (see the Supporting Information). These observations are similar to those previously seen for KIV_6 (*27*) and KIV_{10} (*30*). The only notable difference between affected residues in KIV_7 and KIV_8 involves Thr[21] and Cys[22] in each module. The backbone H^N groups of these residues in KIV_7 displayed chemical-shift changes greater than the average chemical-shift change, while those in KIV_8 did not. In both structures, Cys[22] forms a disulfide bridge with Cys[61], which borders the LBS, and likely results in ϵ-ACA-induced conformational effects being transmitted through covalent linkage. While notable, this difference appears to be subtle because the observed chemical-shift changes for Thr[21] and Cys[22] in KIV_7 are slightly greater than the average chemical-shift change, while chemical-shift changes for these residues in KIV_8 are slightly below the average chemical-shift change.

To assess ligand specificity, intrinsic tryptophan fluorescence was used to monitor the binding of apo(a) KIV_8 to ϵ-ACA, lysine, arginine, and proline, which are molecules that have previously been shown to inhibit noncovalent interactions between a recombinant 17-kringle form of apo(a) and immobilized LDL (*15*). Apo(a) KIV_8 preferentially binds ϵ-ACA, with a K_d of 655 μM, compared to K_d values of 5.75 and 7.30 mM for L-arginine and L-lysine, respectively (Table 2). When the affinities determined for apo(a) KIV_8 were compared to a parallel experiment involving apo(a) KIV_7, which gave rise to K_d values of 291 μM, 2.55 mM, and 2.49 mM for ϵ-ACA, L-arginine, and L-lysine, respectively, they were found to be 2−3-fold weaker. These observed K_d values for apo(a) KIV_7 are similar to those previously determined for apo(a) KIV_7 (*12*, *31*), with the exception of the K_d values for arginine and proline. Our value of 2.49 ± 0.4 mM for arginine is significantly less than the value of 6.7 ± 1.1 mM reported by Rahman et al., and we could not detect a fluorescence change upon titration of proline, whereas a K_d value of 4.5 mM for proline was previously determined (*31*). These differences could be attributed to our modified purification protocol in which we have included an additional HPLC purification step to remove residual ions.

DISCUSSION

The weak lysine-binding apo(a) kringle modules KIV_7 and KIV_8 display a 2−3-fold difference in affinity for lysine and lysine analogues, and recently, each has been shown to regulate the noncovalent step in Lp(a) assembly through recognition of unique lysine-containing sequences within apoB-100 (*12*). These differences occur despite the fact that they share 84% sequence identity, including conservation

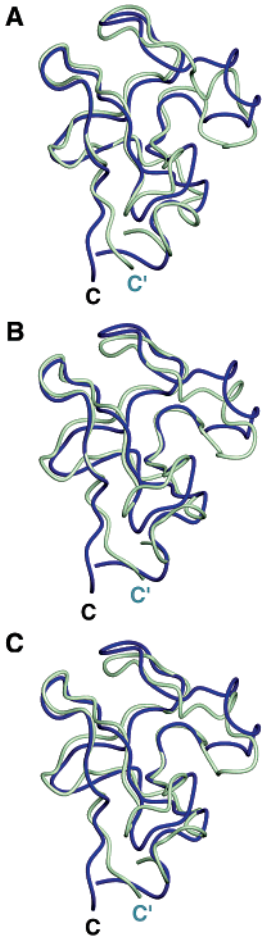

FIGURE 5: Backbone superposition of apo(a) KIV_8 (blue) with (A) apo(a) KIV_6, (B) apo(a) KIV_7, and (C) apo(a) KIV_{10}. The backbone traces of the KIV_6 (*27*), KIV_7 (*32*), and KIV_{10} (*29*) modules are depicted in gray, and their C terminus is labeled C′. The C terminus of apo(a) KIV_8 is labeled C. Alignment included residues Cys[1]−Cys[78] and was performed in MOLMOL (*53*).

of the cationic center (Arg[35] and Arg[69]), anionic center (Asp[54] and Glu[56]), and hydrophobic center (Trp[60], Tyr[62], Trp[70], and Tyr[72]) of the LBS (*4*), which was first identified in the plasminogen kringle 4 module (*59*). In the present work, we have determined the solution structure of KIV_8, characterized its dynamic properties, and used NMR spectroscopy to monitor the residue-specific effects of ϵ-ACA binding on KIV_7 and KIV_8 in an attempt to identify the structural basis for the observed differences in ligand affinity and specificity.

Comparison to Existing Kringle Module Structures. Three-dimensional structures exist for the strong lysine-binding apo(a) KIV_{10} module (*29*, *30*) and the weak lysine-binding apo(a) KIV_6 (*27*) and KIV_7 (*32*) modules. While the KIV_8 structure described here shares a similar overall fold with these structures (Figure 5), backbone pairwise rmsd values of 2.60, 2.71, and 2.56 Å for KIV_8 with KIV_6, KIV_7, and KIV_{10}, respectively, are significantly higher than those previously reported for the comparison of the C_α traces of KIV_6 with KIV_7 (1.64 Å) and KIV_{10} (1.50 Å) (*27*) and KIV_7 with KIV_{10} (0.5 Å) (*32*). Conspicuous differences between the backbone conformations of KIV_8 and the other apo(a) kringle modules reside in the N and C termini and within a loop and turn comprising residues 34−45. The relaxation parameters for residues located in the N and C termini of the core region of KIV_8 and the temperature factors for the analogous regions

in the KIV_7 crystal structure indicated that they are well-ordered in both modules, ruling out a dynamics-based rationale for the observed structural differences.

A hydrogen-bonding network involving Arg^{35}, Tyr^{40}, and Asp^{54} in the KIV_7 crystal structure was previously suggested to play a role in the reduced lysine-binding affinity by restricting the adaptability of the cationic and anionic centers of the LBS to accommodate the ligand (*32*). An analogous hydrogen-bonding network is not observed in our KIV_8 solution structure. Rather, Tyr^{40} forms extensive hydrophobic contacts with Pro^{37}, Ala^{43}, and Leu^{45} in KIV_8, leading to a ~180° difference in orientation of the Tyr^{40} aromatic ring, when compared to its position in KIV_7 (*32*). Because this conformational deviation restricts Tyr^{40} from participating in such a hydrogen-bonding network in KIV_8, the underlying structural basis for the observed weak lysine affinity must be unique from that of KIV_7. Interestingly, the weak LBS of KIV_6 has similar hydrophobic and anionic center conformations to those of KIV_7, displays similar affinities for lysine analogues to KIV_7, yet is also lacking the analogous hydrogen-bonding network (*27*, *32*).

Arg^{35} is a key residue in the cationic center of the LBS and occupies a central position within the LBS of KIV_7 because of hydrogen-bonding contacts with Tyr^{40} and Tyr^{62} (*32*). In contrast, the side chain of Arg^{35} is fully exposed to the solvent and 6.4 Å from the aromatic ring of Tyr^{62} in KIV_8, a residue previously shown to be important for LDL binding by KIV_7 (*14*). The position of Arg^{35} relative to the LBS in KIV_8 suggests that a backbone conformational change would have to accompany lysine binding for the side chain of Arg^{35} to participate at the cationic center. Crystal structures of KIV_{10} in the apo and ligand-bound states indicate that the LBS is preformed and that no significant conformational changes accompany ligand binding (*29*, *30*). In the case of KIV_6, a lack of a detectable backbone H^N resonance for Arg^{35} led the authors to suggest that this is a region of high flexibility, which could accommodate such a change without distorted proximal regions of the module (*27*). We were also unable to identify the backbone H^N resonance of Arg^{35} for both KIV_7 and KIV_8. However, our relaxation parameters show that the region surrounding Arg^{35} is well-ordered in KIV_8, which suggests that the lack of an identifiable backbone H^N resonance is due to this group not participating in a hydrogen bond and at the same time being accessible to the solvent. The KIV_8 structure and relaxation parameters suggest that a significant change in the backbone conformation would have to occur for Arg^{35} to optimally participate in the LBS. Given that the KIV_7 structure is similar to the apo and complexed KIV_{10} structures (*32*) and that our chemical-shift mapping studies of KIV_7 and KIV_8 indicate that ϵ-ACA binding induces a similar and limited backbone conformational change in both modules, these observations suggest that the preformed conformation of the KIV_8 LBS is not optimal for ligand binding, thereby resulting in a lower affinity for lysine compared to KIV_7. Note, with the exception of Asn, Gln, and Trp side-chain amide groups, the extent of side-chain reorientations within the LBS of KIV_8 cannot be determined from the presented chemical-shift mapping data.

Inspection of the LBS beyond Arg^{35} revealed a substantial alteration in the orientation of tryptophan (Trp^{60} and Trp^{70}) and tyrosine (Tyr^{62} and Tyr^{72}) residues that comprise the hydrophobic center, when compared to KIV_6, KIV_7, and KIV_{10} (Figure 6). The aromatic rings of Tyr^{62} and Tyr^{72} in KIV_8 are rotated clockwise 85° and 15°, respectively, when compared to the analogous residues in KIV_7 and looking down on the LBS. The indole rings of Trp^{60} and Trp^{70} of KIV_8 have moved from a vertical stacking position in KIV_7, where the plane of the rings aligns with the two β strands that form the base of the LBS, to an almost horizontal position, in which the plane of the rings has been rotated almost 90° (Figure 6). The positioning of the indole ring of Trp^{70} in KIV_8 appears to cap the hydrophobic cleft of the LBS, potentially reducing the hydrophobic contacts accessible to ϵ-ACA through steric hindrance, thereby contributing to the 2−3-fold decrease in ligand affinity that we and others have observed for KIV_8 (*12*).

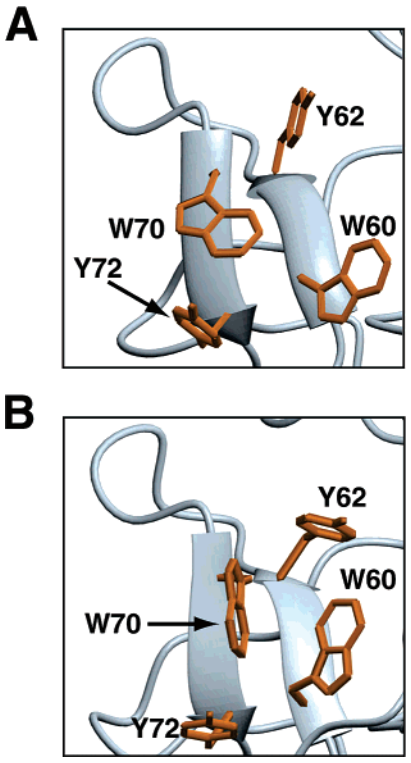

FIGURE 6: Side-chain orientations of aromatic residues defining the hydrophobic center of the LBS in (A) apo(a) KIV_8 and (B) apo(a) KIV_7 (*32*). The side chains are depicted as orange sticks on a gray ribbon backbone diagram. Residues are labeled using a one-letter code for amino acid type, followed by their numerical position in sequence of the construct.

Additional Ligand-Binding Sites. The observation that kringle modules have substantial sequence identity (>80%) yet display unique ligand affinities and specificities suggests that the binding sites encompass molecular determinants beyond the LBS. Analysis of the apo(a) KIV_8 structure reveals an exposed hydrophobic surface formed by residues Met^{28}, Thr^{29}, Trp^{32}, Ile^{36}, Leu^{38}, and Tyr^{39}, which sits adjacent the cationic center (Arg^{35} and Arg^{69}) of the LBS. Of the residues listed, Met^{28}, Thr^{29}, Trp^{32}, and Tyr^{39} are conserved among KIV_6, KIV_7, and KIV_8. The threonine and glutamate residues at positions 36 and 38 of both KIV_6 and KIV_7 are substituted for isoleucine and leucine residues in KIV_8. These differences, particularly at position 38, where there is a hydrophobic versus charged residue, may provide a discrete yet critical mechanism by which KIV_7 and KIV_8 can discriminate between their cognate apoB-100 binding sites

through recognition of residues adjacent to their respective core lysine residue.

KIV_8 contains the sole RGD motif within uncomplexed apo(a) and in the Lp(a) particle. Recent studies, using an apo(a) RGD epitope, have suggested that this motif is responsible for Lp(a)-mediated inhibition of platelet aggregation through binding to the IIb subunit of the fibrinogen receptor (*34*). The RGD motif is located within a solvent-exposed loop at the N terminus of KIV_8 ($Arg^3-Gly^4-Asp^5$) and forms a short β turn containing a hydrogen bond between the backbone carbonyl oxygen of Arg^3 and the backbone amide proton of Asp^5. The structure is similar to the distorted type-II turn formed by the RGD motif from the 10th fibronectin type-III module of fibronectin (*60*). Future biochemical, biophysical, and structural studies of the RGD-mediated interaction between KIV_8 and the fibrinogen receptor will provide unique insight into additional roles for KIV_8 in apo(a) function.

ACKNOWLEDGMENT

We thank Kim Munro of the Protein Function Discovery facility at Queen's University for assisting in the collection of the intrinsic fluorescence data. We thank Stéphane Gagné and Pierre-Yves Savard (Université Laval) and the Québec/Eastern Canada High Field NMR Facility (McGill University) for their technical assistance and use of facilities. We thank Frank Delaglio and Bruce Johnson for providing NMRPipe and NMRView software.

SUPPORTING INFORMATION AVAILABLE

Overlay of 2D $^1H-^{15}N$ HSQC spectra of ^{15}N-KIV_7 in the presence of increasing amounts of ϵ-ACA (Supporting Figure 1) and overlay of 2D $^1H-^{15}N$ HSQC spectra of ^{15}N-KIV_8 in the presence of increasing amounts of ϵ-ACA (Supporting Figure 2). This material is available free of charge via the Internet at http://pubs.acs.org.

REFERENCES

1. Brunner, C., Kraft, H. G., Utermann, G., and Muller, H. J. (1993) Cys4057 of apolipoprotein(a) is essential for lipoprotein(a) assembly, *Proc. Natl. Acad. Sci. U.S.A. 90*, 11643−11647.
2. Koschinsky, M. L., Cote, G. P., Gabel, B., and van der Hoek, Y. Y. (1993) Identification of the cysteine residue in apolipoprotein-(a) that mediates extracellular coupling with apolipoprotein B-100, *J. Biol. Chem. 268*, 19819−19825.
3. Fless, G. M., ZumMallen, M. E., and Scanu, A. M. (1986) Physicochemical properties of apolipoprotein(a) and lipoprotein-(a-) derived from the dissociation of human plasma lipoprotein (a), *J. Biol. Chem. 261*, 8712−8718.
4. McLean, J. W., Tomlinson, J. E., Kuang, W. J., Eaton, D. L., Chen, E. Y., Fless, G. M., Scanu, A. M., and Lawn, R. M. (1987) cDNA sequence of human apolipoprotein(a) is homologous to plasminogen, *Nature 330*, 132−137.
5. Lackner, C., Cohen, J. C., and Hobbs, H. H. (1993) Molecular definition of the extreme size polymorphism in apolipoprotein-(a), *Hum. Mol. Genet. 2*, 933−940.
6. van der Hoek, Y. Y., Wittekoek, M. E., Beisiegel, U., Kastelein, J. J., and Koschinsky, M. L. (1993) The apolipoprotein(a) kringle IV repeats which differ from the major repeat kringle are present in variably-sized isoforms, *Hum. Mol. Genet. 2*, 361−366.
7. Marcovina, S. M., and Koschinsky, M. L. (2002) A critical evaluation of the role of Lp(a) in cardiovascular disease: Can Lp(a) be useful in risk assessment? *Semin. Vasc. Med. 2*, 335−344.
8. Koschinsky, M. L., and Marcovina, S. M. (2004) Structure−function relationships in apolipoprotein(a): Insights into lipoprotein(a) assembly and pathogenicity, *Curr. Opin. Lipidol. 15*, 167−174.
9. Boffa, M. B., Marcovina, S. M., and Koschinsky, M. L. (2004) Lipoprotein(a) as a risk factor for atherosclerosis and thrombosis: Mechanistic insights from animal models, *Clin. Biochem. 37*, 333−343.
10. Catena, C., Novello, M., Lapenna, R., Baroselli, S., Colussi, G., Nadalini, E., Favret, G., Cavarape, A., Soardo, G., and Sechi, L. A. (2005) New risk factors for atherosclerosis in hypertension: Focus on the prothrombotic state and lipoprotein(a), *J. Hypertens. 23*, 1617−1631.
11. Koschinsky, M. L. (2005) Lipoprotein(a) and atherosclerosis: New perspectives on the mechanism of action of an enigmatic lipoprotein, *Curr. Atheroscler. Rep. 7*, 389−395.
12. Becker, L., Cook, P. M., Wright, T. G., and Koschinsky, M. L. (2004) Quantitative evaluation of the contribution of weak lysine-binding sites present within apolipoprotein(a) kringle IV types 6−8 to lipoprotein(a) assembly, *J. Biol. Chem. 279*, 2679−2688.
13. Becker, L., McLeod, R. S., Marcovina, S. M., Yao, Z., and Koschinsky, M. L. (2001) Identification of a critical lysine residue in apolipoprotein B-100 that mediates noncovalent interaction with apolipoprotein(a), *J. Biol. Chem. 276*, 36155−36162.
14. Caterer, N. R., Graversen, J. H., Jacobsen, C., Moestrup, S. K., Sigurskjold, B. W., Etzerodt, M., and Thogersen, H. C. (2002) Specificity determinants in the interaction of apolipoprotein(a) kringles with tetranectin and LDL, *Biol. Chem. 383*, 1743−1750.
15. Gabel, B. R., and Koschinsky, M. L. (1998) Sequences within apolipoprotein(a) kringle IV types 6−8 bind directly to low-density lipoprotein and mediate noncovalent association of apolipoprotein-(a) with apolipoprotein B-100, *Biochemistry 37*, 7892−7898.
16. Trieu, V. N., and McConathy, W. J. (1998) Functional characterization of T7 and T8 of human apolipoprotein (a), *Biochem. Biophys. Res. Commun. 251*, 356−359.
17. Guevara, J., Jr., Spurlino, J., Jan, A. Y., Yang, C. Y., Tulinsky, A., Prasad, B. V., Gaubatz, J. W., and Morrisett, J. D. (1993) Proposed mechanisms for binding of apo[a] kringle type 9 to apo B-100 in human lipoprotein[a], *Biophys. J. 64*, 686−700.
18. Guevara, J., Jr., Valentinova, N. V., Garcia, O., Gotto, A. M., Yang, C. Y., Legal, S., Gaubatz, J., and Sparrow, J. T. (1996) Interaction of apolipoprotein[a] with apolipoproteinB-100 Cys3734 region in lipoprotein[a] is confirmed immunochemically, *J. Protein Chem. 15*, 17−25.
19. Callow, M. J., and Rubin, E. M. (1995) Site-specific mutagenesis demonstrates that cysteine 4326 of apolipoprotein B is required for covalent linkage with apolipoprotein (a) in vivo, *J. Biol. Chem. 270*, 23914−23917.
20. McCormick, S. P., Ng, J. K., Taylor, S., Flynn, L. M., Hammer, R. E., and Young, S. G. (1995) Mutagenesis of the human apolipoprotein B gene in a yeast artificial chromosome reveals the site of attachment for apolipoprotein(a), *Proc. Natl. Acad. Sci. U.S.A. 92*, 10147−10151.
21. Frank, S., Durovic, S., Kostner, K., and Kostner, G. M. (1995) Inhibitors for the in vitro assembly of Lp(a), *Arterioscler., Thromb., Vasc. Biol. 15*, 1774−1780.
22. Gabel, B. R., May, L. F., Marcovina, S. M., and Koschinsky, M. L. (1996) Lipoprotein(a) assembly. Quantitative assessment of the role of apo(a) kringle IV types 2−10 in particle formation, *Arterioscler., Thromb., Vasc. Biol. 16*, 1559−1567.
23. Koschinsky, M. L., and Marcovina, S. M. (1997) Lipoprotein(a): Structural implications for pathophysiology, *Int. J. Clin. Lab. Res. 27*, 14−23.
24. Ernst, A., Helmhold, M., Brunner, C., Petho-Schramm, A., Armstrong, V. W., and Muller, H. J. (1995) Identification of two functionally distinct lysine-binding sites in kringle 37 and in kringles 32−36 of human apolipoprotein(a), *J. Biol. Chem. 270*, 6227−6234.
25. Gabel, B. R., McLeod, R. S., Yao, Z., and Koschinsky, M. L. (1998) Sequences within the amino terminus of ApoB100 mediate its noncovalent association with apo(a), *Arterioscler., Thromb., Vasc. Biol. 18*, 1738−1744.
26. Trieu, V. N., and McConathy, W. J. (1995) A two-step model for lipoprotein(a) formation, *J. Biol. Chem. 270*, 15471−15474.
27. Maderegger, B., Bermel, W., Hrzenjak, A., Kostner, G. M., and Sterk, H. (2002) Solution structure of human apolipoprotein(a) kringle IV type 6, *Biochemistry 41*, 660−668.

28. LoGrasso, P. V., Cornell-Kennon, S., and Boettcher, B. R. (1994) Cloning, expression, and characterization of human apolipoprotein-(a) kringle IV37, *J. Biol. Chem. 269*, 21820−21827.
29. Mikol, V., LoGrasso, P. V., and Boettcher, B. R. (1996) Crystal structures of apolipoprotein(a) kringle IV37 free and complexed with 6-aminohexanoic acid and with *p*-aminomethylbenzoic acid: Existence of novel and expected binding modes, *J. Mol. Biol. 256*, 751−761.
30. Mochalkin, I., Cheng, B., Klezovitch, O., Scanu, A. M., and Tulinsky, A. (1999) Recombinant kringle IV-10 modules of human apolipoprotein(a): Structure, ligand binding modes, and biological relevance, *Biochemistry 38*, 1990−1998.
31. Rahman, M. N., Becker, L., Petrounevitch, V., Hill, B. C., Jia, Z., and Koschinsky, M. L. (2002) Comparative analyses of the lysine binding site properties of apolipoprotein(a) kringle IV types 7 and 10, *Biochemistry 41*, 1149−1155.
32. Ye, Q., Rahman, M. N., Koschinsky, M. L., and Jia, Z. (2001) High-resolution crystal structure of apolipoprotein(a) kringle IV type 7: Insights into ligand binding, *Protein Sci. 10*, 1124−1129.
33. Sotiriou, S. N., Orlova, V. V., Al-Fakhri, N., Ihanus, E., Economopoulou, M., Isermann, B., Bdeir, K., Nawroth, P. P., Preissner, K. T., Gahmberg, C. G., Koschinsky, M. L., and Chavakis, T. (2006) Lipoprotein(a) in atherosclerotic plaques recruits inflammatory cells through interaction with Mac-1 integrin, *FASEB J. 20*, 559−561.
34. Barre, D. E. (2006) Arginyl−glycyl−aspartyl (RGD) epitope of human apolipoprotein (a) inhibits platelet aggregation by antagonizing the IIb subunit of the fibrinogen (GPIIb/IIIa) receptor, *Thromb. Res.*, in press.
35. Kay, L., Keifer, P., and Saarinen, T. (1992) Pure absorption gradient enhanced heteronuclear single quantum correlation spectroscopy with improved sensitivity, *J. Am. Chem. Soc. 114*, 10663−10665.
36. Wittekind, M., and Mueller, L. (1993) HNCACB, a high-sensitivity 3D NMR experiment to correlate amide-proton and nitrogen resonances with the α- and β-carbon resonances, *J. Magn. Reson., Ser. B 101*, 171−180.
37. Grzesiek, S., and Bax, A. (1993) Amino acid type determination in the sequential assignment procedure of uniformly $^{13}C/^{15}N$-enriched proteins, *J. Biomol. NMR 3*, 185−204.
38. Kuboniwa, H., Grzesiek, S., Delaglio, F., and Bax, A. (1994) Measurement of H^N-H^α *J* couplings in calcium-free calmodulin using new 2D and 3D water-flip-back methods, *J. Biomol. NMR 4*, 871−878.
39. Vuister, G. W., and Bax, A. (1994) Measurement of four-bond H^N-H^α *J*-couplings in staphylococcal nuclease, *J. Biomol. NMR 4*, 193−200.
40. Muhandiram, D. R., and Kay, L. E. (1994) Gradient-enhanced triple-resonance three-dimensional NMR experiments with improved sensitivity, *J. Magn. Reson., Ser. B 103*, 203−216.
41. Kay, L., Xu, G., Singer, A., Muhandiram, D., and Forman-Kay, J. (1993) A gradient-enhanced HCCH−TOCSY experiment for recording side-chain ^1H and ^{13}C correlations in H_2O samples of proteins, *J. Magn. Reson., Ser. B 101*, 333−337.
42. Zhang, O., Kay, L. E., Olivier, J. P., and Forman-Kay, J. D. (1994) Backbone ^1H and ^{15}N resonance assignments of the N-terminal SH3 domain of drk in folded and unfolded states using enhanced-sensitivity pulsed field gradient NMR techniques, *J. Biomol. NMR 4*, 845−858.
43. Pascal, S. M., Muhandiram, D. R., Yamazaki, T., Forman-Kay, J. D., and Kay, L. E. (1994) Simultaneous acquisition of ^{15}N- and ^{13}C-edited NOE spectra of proteins dissolved in H_2O, *J. Magn. Reson., Ser. B 103*, 197−201.
44. Schleucher, J., Schwendinger, M., Sattler, M., Schmidt, P., Schedletzky, O., Glaser, S. J., Sorensen, O. W., and Griesinger, C. (1994) A general enhancement scheme in heteronuclear multidimensional NMR employing pulsed field gradients, *J. Biomol. NMR 4*, 301−306.
45. Delaglio, F., Grzesiek, S., Vuister, G. W., Zhu, G., Pfeifer, J., and Bax, A. (1995) NMRPipe: A multidimensional spectral processing system based on UNIX pipes, *J. Biomol. NMR 6*, 277−293.
46. Johnson, B. A. (2004) Using NMRView to visualize and analyze the NMR spectra of macromolecules, *Methods Mol. Biol. 278*, 313−352.
47. Farrow, N. A., Zhang, O., Forman-Kay, J. D., and Kay, L. E. (1994) A heteronuclear correlation experiment for simultaneous determination of ^{15}N longitudinal decay and chemical exchange rates of systems in slow equilibrium, *J. Biomol. NMR 4*, 727−734.
48. Palmer, A. G., III (1997) Probing molecular motion by NMR, *Curr. Opin. Struct. Biol. 7*, 732−737.
49. Brunger, A. T., Adams, P. D., Clore, G. M., DeLano, W. L., Gros, P., Grosse-Kunstleve, R. W., Jiang, J. S., Kuszewski, J., Nilges, M., Pannu, N. S., Read, R. J., Rice, L. M., Simonson, T., and Warren, G. L. (1998) Crystallography & NMR system: A new software suite for macromolecular structure determination, *Acta Crystallogr., Sect. D: Biol. Crystallogr. 54* (part 5), 905−921.
50. Cornilescu, G., Delaglio, F., and Bax, A. (1999) Protein backbone angle restraints from searching a database for chemical shift and sequence homology, *J. Biomol. NMR 13*, 289−302.
51. Vuister, G. W., Yamazaki, T., Torchia, D. A., and Bax, A. (1993) Measurement of two- and three-bond $^{13}C-^1H$ *J* couplings to the C_δ carbons of leucine residues in staphylococcal nuclease, *J. Biomol. NMR 3*, 297−306.
52. Laskowski, R., MacArthur, M., Moss, D., and Thornton, J. (1993) PROCHECK: A program to check the stereochemical quality of protein structures, *J. Appl. Crystallogr. 26*, 283−291.
53. Koradi, R., Billeter, M., and Wuthrich, K. (1996) MOLMOL: A program for display and analysis of macromolecular structures, *J. Mol. Graphics 14*, 29−32, 51−55.
54. DeLano, W. L. (2002) *The PyMOL Molecular Graphics System*, DeLano Scientific, San Carlos, CA.
55. Zajicek, J., Chang, Y., and Castellino, F. J. (2000) The effects of ligand binding on the backbone dynamics of the kringle 1 domain of human plasminogen, *J. Mol. Biol. 301*, 333−347.
56. Kay, L. E., Torchia, D. A., and Bax, A. (1989) Backbone dynamics of proteins as studied by ^{15}N inverse detected heteronuclear NMR spectroscopy: Application to staphylococcal nuclease, *Biochemistry 28*, 8972−8979.
57. Hansen, A. P., Petros, A. M., Meadows, R. P., and Fesik, S. W. (1994) Backbone dynamics of a two-domain protein: ^{15}N relaxation studies of the amino-terminal fragment of urokinase-type plasminogen activator, *Biochemistry 33*, 15418−15424.
58. Marti, D. N., Schaller, J., and Llinas, M. (1999) Solution structure and dynamics of the plasminogen kringle 2-AMCHA complex: 3(1)-helix in homologous domains, *Biochemistry 38*, 15741−15755.
59. Nielsen, P. R., Einer-Jensen, K., Holtet, T. L., Andersen, B. D., Poulsen, F. M., and Thogersen, H. C. (1993) Protein−ligand interactions in the lysine-binding site of plasminogen kringle 4 are different in crystal and solution. Electrostatic interactions studied by site-directed mutagenesis exclude Lys35 as an important acceptor in solution, *Biochemistry 32*, 13019−13025.
60. Leahy, D. J., Aukhil, I., and Erickson, H. P. (1996) 2.0 Å crystal structure of a four-domain segment of human fibronectin encompassing the RGD loop and synergy region, *Cell 84*, 155−164.
61. Farmer, B. T., II, Constantine, K. L., Goldfarb, V., Friedrichs, M. S., Wittekind, M., Yanchunas, J., Jr., Robertson, J. G., and Mueller, L. (1996) Localizing the $NADP^+$ binding site on the MurB enzyme by NMR, *Nat. Struct. Biol. 3*, 995−997.

BI061814G